Unusual Slow Magnetic Relaxation in Helical $Co_3(OH)_2$ Ferrimagnetic Chain Based Cobalt Hydroxysulfates

Xian-Ming Zhang,*,† Cui-Rui Li,† Xu-Hui Zhang,† Wei-Xiong Zhang,‡ and Xiao-Ming Chen‡

School of Chemistry & Material Science, Shanxi Normal University, Linfen 041004, P. R. China, MOE Key Laboratory of Bioinorganic and Synthetic Chemistry, School of Chemistry and Chemical Engineering, Sun Yat-Sen University, Guangzhou 510275, P. R. China

Received November 15, 2007. Revised Manuscript Received January 2, 2008

Two cobalt hydroxysulfates $Na_2Co_3(OH)_2(SO_4)_3(H_2O)_4$ (**1**) and $Co_3(OH)_2(HSO_4)_2(SO_4)(H_2O)_4$ (**2**) have been prepared and characterized by single-crystal X-ray diffraction, thermal analysis, and magnetic measurements. The structure of **1** consists of helical $Co_3(OH)_2$ ferrimagnetic chains that are connected by μ_3- and μ_4-sulfates into a two-dimensional anionic $[Co_3(OH)_2(SO_4)_3(H_2O)_2]^{2-}$ layer. The adjacent $[Co_3(OH)_2(SO_4)_2(H_2O)_2]^{2-}$layers in **1** are further linked by Na^+ ions into a three-dimensional framework. The related compound **2** also consists of helical $Co_3(OH)_2$ ferrimagnetic chains but has a two-dimensional layered structure due to the absence of Na^+ ions and partial replacement of sulfates by hydrosulfates. Preliminary magnetic measurements show that **1** and **2** have similar behavior. A detailed magnetic study of **1** reveals a stepped hysteresis loop at 2 K with a coercive field of 1800 Oe and remnant magnetization of 2.8 $N\beta$ attributed to the different anisotropy axes of Co(II) spins in the helical $Co_3(OH)_2$ chain. Field-cooled (FC) and zero-field-cooled (ZFC) magnetization measurements show that **1** has a blocking temperature ca 28 K. The study of frequency dependence of real χ_m' component of ac susceptibility by the equation $\varphi = \Delta T_f/[T_f\Delta(\log \omega]$ exhibits that **1** is close to a spin glass. The fitting of Arrhenius law reveals that τ_0 seems a little longer but the U/k_B is normal for a typical single-chain magnet following Glauber dynamics. The $-z\nu$ value of 3.3 obtained by the conventional critical scaling law of the spin dynamics $\tau = \tau_0 (T_p - T_f/T_f)^{-z\nu}$ is out of the range for various spin glasses. The plot of $d\log(T)/d\log(\chi T)_{ferro}$ versus T eliminates the phase transition to long-range ordering and suggests that **1** is a real one-dimensional system. The unusual slow magnetic relaxation behavior of **1** is tentatively ascribed to be a ferrimagnetic chain with spin-glass-like dynamic relaxation, possibly arising from the movement of the domain walls.

Introduction

One-dimensional magnetic compounds, especially showing single-chain magnetic properties, are currently of ongoing interest for the design and synthesis of new molecule-based magnets.[1] The creation of single-chain magnets (SCMs) arose from Glauber's theoretical work in which he suggested that the conditions to be fulfilled to observe slow magnetic relaxation in a one-dimensional compound were as follows: (i) it must behave as an Ising ferro- or ferrimagnetic chain and (ii) the ratio J/J' has to be larger than 1×10^4 (J and J' being the intrachain and interchain magnetic interactions, respectively).[2]The slow magnetic relaxation and a hysteresis loop in SCMs below the blocking temperature make them good candidates for potential high-density information storage in low-dimensional materials. Well-documented examples of single-chain magnets include $[Co(hfacac)_2(NITPhOMe)]$,[3,4] $[Dy(hfac)_3\{NIT(C_6H_4OPh)\}]$,[5] (hfacac = hexafluoroacetylacetonate; NIT(R) = 2-(4′-R)-4,4,5,5-tetramethylimidazoline-1-oxyl-3-oxide), $[Co(2,2'\text{-bithiazoline})(N_3)_2]$ (bt = 2,2′-bithiazoline),[6] $[Mn_2(saltmen)_2\text{-}Ni(pao)_2L_2](A)_2$ (saltmen = *N*,*N*′−1,1,2,2-tetramethylethylenebis(salicylideneiminate), pao = pyridine-2-aldoximate, and *A* = anion),[7,8] $[(Tp)_2Fe_2(CN)_6Cu(CH_3OH)\cdot 2CH_3OH]_n$ (Tp = Tris(pyrazolyl)hydroborate),[9] *catena*-$[Fe(ClO_4)_2\{Fe(bpca)_2\}]ClO_4$ (Hbpca = bis-(2-pyridylcarbonyl)amine),[10] $[CoCu(2,4,6\text{-tmpa})_2(H_2O)_2]\cdot 4H_2O$,[11] $[Mn_7O_8(O_2SePh)_8(O_2CMe)(H_2O)]$,[12] and $[Mn_3O(t\text{Bu-sao})_3(HCOO)(CH_3OH)_4]\cdot CH_3OH\cdot 0.5H_2O$ (*t*Bu-saoH$_2$

* Corresponding author. Tel & Fax: +86 357 2051402. E-mail: zhangxm@dns.sxnu.edu.cn.
† Shanxi Normal University.
‡ Yat-Sen University.

(1) Lescouezec, R.; Tomaa, L. M.; Vaissermann, J.; Verdaguer, M.; Delgado, F. S.; Ruiz-Perez, C.; Lloret, F.; Julve, M. *Coord. Chem. Rev.* **2005**, *249*, 2691.
(2) Glauber, R. J. *J. Math. Phys.* **1963**, *4*, 294.
(3) Caneschi, A.; Gatteschi, D.; Lalioti, N.; Sangregorio, C.; Sessoli, R.; Venturi, G.; Vindigni, A.; Rettori, A.; Pini, M. G.; Novak, M. A. *Angew. Chem., Int. Ed.* **2001**, *40*, 1760.
(4) Caneschi, A.; Gatteschi, D.; Lalioto, N.; Sessoli, R.; Sorace, L.; Tangoulis, V.; Vindigni, A. *Chem.—Eur. J.* **2002**, *8*, 286.
(5) Bogani, L.; Sangregorio, C.; Sessoli, R.; Gatteschi, D. *Angew. Chem., Int. Ed.* **2005**, *44*, 5817.
(6) Liu, T.-F.; Fu, D.; Gao, S.; Zhang, Y.-Z.; Sun, H.-L.; Su, G.; Liu, Y.-J. *J. Am. Chem. Soc.* **2003**, *125*, 13976.
(7) Clérac, R.; Miyasaka, H.; Yamashita, M.; Coulon, C. *J. Am. Chem. Soc.* **2002**, *124*, 12837.
(8) Miyasaka, H.; Clerac, R.; Mizushima, K.; Sugiura, K. I.; Yamashita, M.; Wernsdorfer, W.; Coulon, C. *Inorg. Chem.* **2003**, *42*, 8203.
(9) Wang, S.; Zuo, J.-L.; Gao, S.; Song, Y.; Zhou, H.-C.; Zhang, Y.-Z.; You, X.-Z. *J. Am. Chem. Soc.* **2004**, *126*, 8900.
(10) Kajiwara, T.; Nakano, M.; Kaneko, Y.; Takaishi, S.; Ito, T.; Yamashita, M.; Igashira-Kamiyama, A.; Nojiri, H.; Ono, Y.; Kojima, N. *J. Am. Chem. Soc.* **2005**, *127*, 10150.
(11) Pardo, E.; Bernot, K.; Julve, M.; Lloret, F.; Cano, J.; Ruiz-Garcıa, R.; Pasan, J.; Ruiz-Perez, C.; Ottenwaelder, X.; Journaux, Y. *Chem. Commun.* **2004**, 920.

10.1021/cm7032542 CCC: $40.75
Published on Web 02/21/2008

= 3,5-ditert-butylsalicylaldoxime).[13] Interestingly, some two- and three-dimensional frameworks such as $[Co_3(OH)_2(trans\text{-}1,2\text{-chdc})_2]_n$ (*trans*-1,2-chdc = *trans*-1,2-cyclohexanedicarboxylate),[14] $[Co_3(OH)_2(bime)_2(HO\text{-}BDC)_2]_n$ (bime = 1,2-bis(imidazolyl)ethane, HO-BDC = 5-hydroxyisophthalate),[15] and $[Co_3(OH)_2(btca)_2]\cdot 3.7H_2O$ (btca=benzotriazole-5-carboxylate)[16] also show SCM-like behavior. Within these frameworks, Ising magnetic chain building units are separated by solvent molecules, poor electron transmitted σ-bonding linkers or very long π-bonding linkers. It is clear that the anisotropy of the high-spin cobalt often produces a barrier for the orientation of the magnetization. It is worthwhile that the slow magnetic relaxation phenomenon is common to SCMs, single molecule magnets, supermagnets, and spin-glass magnets. In some interesting cases where magnetic behavior shows a transition from a one-dimensional to three-dimensional system, the assignment of magnetic behavior in these cases is obscure. For example, chainlike compound $[Ni(N_3)(bmdt)(N_3)]\cdot$DMF (bmdt = *N*,*N*-bis(4-methoxylbenzyl)-diethylenetriamine) shows a very interesting magnetic behavior between a SCM and a spin glass.[17]

On the other hand, there is reviving interest in cobalt hydroxysulfates to both chemists and physicists because the hydroxides often in μ_3 mode are coordinated to cobalt atoms providing favorable Co−O−Co magnetic exchanges and the sulfates provide weaker exchanges via Co−O−S−O−Co.[18–22] In 2001, Rosseinsky presented two new cobalt hydroxysulfates containing modified brucite-like cobalt−hydroxide layers bridged by ethylenediamine or dabco.[19] They are canted antiferromagnets where the moments within one ferrimagnetic layer oppose those in the neighboring layers and show a further metamagnetic transition at fairly low applied fields. In 2004, Vilminot et al. reported the structure and magnetic properties of a ferromagnetic phase, $Co_5(OH)_6(SO_4)_2(H_2O)_4$, which consists of truly brucite layers bridged by an inorganic $Co(H_2O)_4(SO_4)_2$.[20] Subsequently, the magnetic structures of $Co_5(OH)_6(SO_4)_2(H_2O)_4$ and $Co_3(OH)_2(SO_4)_2(H_2O)_2$ have been determined.[21] In addition, Rao et al. reported an organically templated cobalt sulfate $[H_2N(CH_2)_4NH_2][NH_4]_2[Co_3F_6(SO_4)_2]$ that has frustrated kagome lattice.[22]

The choice of the building block is very important in the design of one-dimensional magnets. To obtain a magnetic ground state, the magnetic chains should be ferromagnetic, ferrimagnetic, or canted antiferromagnetic chains. On our research of porous magnetic metal organic frameworks, we reported ferrimagnetic $Co_3(OH)_2$ chain-based compounds $[Co_3(OH)_2(btca)_2]\cdot 3.7H_2O$ and $[Co_3(OH)_2(btca)_2]$.[16] The role of solvent molecules between magnetic chain building units is highlighted by field-induced metamagnetism of the dehydrated phase $[Co_3(OH)_2(btca)_2]$ and SCM-like behavior of the hydrated phase $[Co_3(OH)_2(btca)_2]\cdot 3.7H_2O$. To further check the influence of different linkers on the magnetic behaviors of $Co_3(OH)_2$ chain-based compounds, we have synthesized two cobalt hydroxysulfates $Na_2Co_3(OH)_2(SO_4)_3(H_2O)_4$ (**1**) and $Co_3(OH)_2(HSO_4)_2(SO_4)(H_2O)_4$ (**2**). The structure of **1** has been suggested[23,24] and the structure of the corresponding K salt has been solved.[25] In **1** and **2**, the intrachain cobalt atoms are linked by μ_3-hydroxides with Co···Co distances of 3.0–3.6 Å, whereas the helical $Co_3(OH)_2$ chains are linked by sulfates in Co−O−S−O−Co fashion with Co···Co distances of 5.5–6.0 Å. Because of poor electronic transmission of σ-bonding sulfates and larger interchain Co···Co distance, the interchain magnetic interaction is expected to be weaker than intrachain interaction, which may provide a chance to study the transition from one-dimensional to three-dimensional magnetic system. We report herein the unusual slow magnetic relaxation in **1**, which contains helical $Co_3(OH)_2$ ferrimagnetic chains linked by sulfates.

Experimental Section

General Remarks. The FT-IR spectra were recorded from KBr pellets in range 400–4000 cm^{-1} on a Nicolet 5DX spectrometer. XRPD data were recorded in a Bruker D8 ADVANCE diffractometer. Thermal analyses were carried out in air using SETARAM LABSYS equipment with a heating rate of 10 °C/min. The magnetic measurements were performed with Quantum Design SQUID MPMS XL-7 instruments. The diamagnetism of the sample and holder were taken into account.

Syntheses. *$Na_2Co_3(OH)_2(SO_4)_3(H_2O)_4$ (**1**).* A mixture of $CoSO_4\cdot 7H_2O$ (0.4 mmol), cyclohexane-1,4-dicarboxylic acid (0.4 mmol), NaOH (1 mmol), water (2 mL), and ethanol (4 mL) in a molar ratio of 1:1:2.5:270:170 was sealed in a 15 mL Teflon-lined stainless container, which was heated to 160 °C and held there for 96 h. After cooling to room temperature, block-like single crystals of **1** (ca. 35%) were obtained. IR (KBr): 3485s, 1719w, 1178s, 930w, 680w.

*$Co_3(OH)_2(HSO_4)_2(SO_4)(H_2O)_4$ (**2**).* A mixture of $CoSO_4\cdot 7H_2O$ (0.4 mmol), hypoxanthine (0.2 mmol), water (2 mL), and acetonitrile (4 mL) in a molar ratio of 1:0.5:270:190 was sealed in a 15 mL Teflon-lined stainless container, which was heated to 140 °C and held there for 96 h. After being cooled to room temperature, blocklike single crystals of **2** (ca. 30%) were obtained. Compounds **1** and **2** can be synthesized in the absence of cyclohexane-1,4-dicarboxylic acid and hypoxanthine but we found that the use of cyclohexane-1,4-dicarboxylic acid in **1** and hypoxanthine in **2** was helpful to obtain single crystals of good quality. IR (KBr): 3441s, 3146s, 1640w, 1400s, 1110m, 617w.

(12) Chakov, N. E.; Wernsdorfer, W.; Abboud, K. A.; Christou, G. *Inorg. Chem.* **2004**, *43*, 5919.
(13) Xu, H.-B.; Wang, B.-W.; Pan, F.; Wang, Z.-M.; Gao, S. *Angew. Chem., Int. Ed.* **2007**, *46*, 7388.
(14) Zheng, Y.-Z.; Tong, M.-L.; Zhang, W.-X.; Chen, X.-M. *Angew. Chem., Int. Ed.* **2006**, *45*, 6310.
(15) Li, X. J.; Wang, X. Y.; Gao, S.; Cao, R. *Inorg. Chem.* **2006**, *45*, 1508.
(16) Zhang, X.-M.; Hao, Z.-M.; Zhang, W.-X.; Chen, X.-M. *Angew. Chem., Int. Ed.* **2007**, *46*, 3456.
(17) Liu, X.-T.; Wang, X.-Y.; Zhang, W.-X.; Cui, P.; Gao, S. *Adv. Mater.* **2006**, *18*, 2852.
(18) Ben Salah, M.; Vilminot, S.; Andre, G.; Bouree-Vigneron, F.; Richard-Plouet, M.; Mhiri, T.; Kurmoo, M. *Chem. Mater.* **2005**, *17*, 2612.
(19) Ben Salah, M.; Vilminot, S.; Andre, G.; Richard-Plouet, M.; Mhiri, T.; Takagi, S.; Kurmoo, M. *J. Am. Chem. Soc.* **2006**, *128*, 7972.
(20) Ben Salah, M.; Vilminot, S.; Richard-Plouet, M.; Andre, G.; Mhirid, T.; Kurmoo, M. *Chem. Commun.* **2004**, 2548.
(21) Rujiwatra, A.; Kepert, C. J.; Claridge, J. B.; Rosseinsky, M. J.; Kumagai, H.; Kurmoo, M. *J. Am. Chem. Soc.* **2001**, *123*, 10584.
(22) Behera, J. N.; Paul, G.; Choudhury, A.; Rao, C. N. R. *Chem. Commun.* **2004**, 456.
(23) Dubler, E.; Oswald, H. R. *Helv. Chim. Acta* **1971**, *54*, 1621.
(24) Dubler, E.; Oswald, H. R. *Helv. Chim. Acta* **1971**, *54*, 1628.
(25) Effenberger, H.; Langhof, H. *Monatsh. Chem.* **1984**, *115*, 165.

Table 1. Crystallographic Data for Compounds 1 and 2

formula	$H_{10}Co_3Na_2O_{18}S_3$	$H_{12}Co_3O_{18}S_3$
fw	617.03	573.07
cryst syst	orthorhombic	orthorhombic
space group	$Cmc2_1$	$Cmc2_1$
a (Å)	19.785(3)	18.250(4)
b (Å)	7.2793(9)	7.5988(16)
c (Å)	9.9663(13)	9.813(2)
V (Å^3)	1435.4(3)	1360.9(5)
Z	4	4
ρ_{calcd} (g cm^{-3})	2.855	2.797
μ (mm^{-1})	4.027	4.179
F(000)	1220	1140
size (mm^3)	0.31 × 0.12 × 0.04	0.18 × 0.07 × 0.04
no. of reflns	3230/1509	2765/1464
T_{max}/T_{min}	0.8555 and 0.3683	0.8506/0.5200
data/params	1509/9/141	1464/9/134
S	1.051	1.020
R_1[a]	0.0281	0.0266
wR_2[b]	0.0705	0.0620
$\Delta\rho_{max}/\Delta\rho_{min}$ (e A^{-3})	0.469 and −0.523	0.406 and −0.607

[a] $R_1 = \Sigma F_o\text{-}F_c/\Sigma F_o$, $wR_2 = [\Sigma w(F_o^2\text{-}F_c^2)^2/\Sigma w(F_o^2)^2]^{1/2}$.

X-ray Crystallography. Data were collected at 298 K on a Bruker Apex diffractometer (Mo Kα, $\lambda = 0.71073$ Å). Lorentz-polarization and absorption corrections were applied. The structures were solved with direct methods and refined with full-matrix least-squares technique (SHELX-97). Analytical expressions of neutral-atom scattering factors were employed, and anomalous dispersion corrections were incorporated. All non-hydrogen atoms were refined anisotropically. The crystallographic data are listed in Table 1; selected bond lengths and bond angles are given in Table 2.

Results and Discussions

Description of Structures. Compound **1** crystallizes in orthorhombic space group $Cmc2_1$ and the asymmetric unit consists of one sodium ion, two Co(II) ions, two hydroxides, one and a half sulfate ions, and two water molecules, as shown in Figure 1a. The Co(1) and S(2) atoms are located in the special positions. The Co(1) site adopts an octahedral geometry, coordinated by two hydroxides and four oxygen atoms from three sulfates. The Co(1)–O distances are in the range of 2.059(5)−2.174(5) Å. The cis and trans O−Co(1)−O angles are in the range of 79.58(17)−97.20(9)° and 165.29(17)−174.40(18)°, respectively. The Co(2) site also adopts an octahedral geometry, coordinated by two hydroxides, three oxygen atoms from three sulfates, and one water molecule. The Co(2)−O distances are in the range of 2.053(4)−2.155(4) Å. The cis and trans O−Co(1)−O angles are in the range of 81.44(14)−101.68(16)° and 169.46(18)−172.73(18)°, respectively. The adjacent $Co(1)O_6$ and $Co(2)O_6$ octahedra are corner-shared, whereas two adjacent $Co(2)O_6$ octahedra are edge-shared. The Co(1)···Co(2) and Co(1)···Co(2g) distances are 3.675 and 3.607 Å, respectively. The Co(2)···Co(2d) distance is 3.122 Å. The Co(1)−O(9)−Co(2), Co(1)−O(9)−Co(2d), Co(1)−O(8)−Co(2g), and Co(1)−O(8)−Co(2 h) angles are 118.93(15), 118.93(15), 125.86(13), and 125.86(13)°, respectively. The Co(2)−O(9)−Co(2d) and Co(2g)−O(8)−Co(2 h) angles are 94.72(18) and 97.96(18)°, respectively. Bond

Table 2. Bond Lengths (Å) and Angles (deg) for 1[a]

Co(1)−O(8)	2.059(5)	S(1)−O(2)	1.472(3)
Co(1)−O(9)	2.066(5)	S(1)−O(1)	1.474(3)
Co(1)−O(2)	2.078(3)	S(1)−O(3)	1.478(4)
Co(1)−O(2d)	2.078(3)	S(2)−O(6d)	1.465(3)
Co(1)−O(5)	2.151(4)	S(2)−O(6)	1.465(3)
Co(1)−O(7e)	2.174(5)	S(2)−O(7)	1.474(5)
Co(2)−O(3)	2.053(4)	S(2)−O(5)	1.476(4)
Co(2)−O(8f)	2.069(3)	Na(1)−O(4a)	2.308(4)
Co(2)−O(9)	2.122(3)	Na(1)−O(6b)	2.351(4)
Co(2)−O(1a)	2.134(4)	Na(1)−O(2W)	2.381(5)
Co(2)−O(6e)	2.138(3)	Na(1)−O(1Wc)	2.393(5)
Co(2)−O(1W)	2.155(4)	Na(1)−O(1c)	2.541(5)
S(1)−O(4)	1.462(3)	Na(1)−O(3c)	2.952(5)
O(8)−Co(1)−O(9)	92.64(18)	O(1a)−Co(2)−O(6e)	81.44(14)
O(8)−Co(1)−O(2)	91.16(11)	O(3)−Co(2)−O(1W)	84.63(15)
O(9)−Co(1)−O(2)	97.20(9)	O(8f)−Co(2)−O(1W)	89.20(16)
O(8)−Co(1)−O(2d)	91.16(11)	O(9)−Co(2)−O(1W)	101.68(16)
O(9)−Co(1)−O(2d)	97.20(9)	O(1a)−Co(2)−O(1W)	88.79(14)
O(2)−Co(1)−O(2d)	165.29(17)	O(6e)−Co(2)−O(1W)	170.22(14)
O(8)-Co(1)-O(5)	92.96(17)	O(4)−S(1)−O(2)	109.46(18)
O(9)-Co(1)-O(5)	174.40(18)	O(4)−S(1)−O(1)	109.6(2)
O(2)−Co(1)−O(5)	82.69(9)	O(2)−S(1)−O(1)	110.3(2)
O(2d)−Co(1)−O(5)	82.69(9)	O(4)-S(1)-O(3)	109.3(2)
O(8)−Co(1)−O(7e)	172.54(16)	O(2)−S(1)−O(3)	110.2(2)
O(9)−Co(1)−O(7e)	94.82(17)	O(1)−S(1)−O(3)	108.0(2)
O(2)−Co(1)−O(7e)	87.90(11)	O(6d)−S(2)−O(6)	108.7(3)
O(2d)−Co(1)−O(7e)	87.90(11)	O(6d)−S(2)−O(7)	110.31(18)
O(5)−Co(1)−O(7e)	79.58(17)	O(6)−S(2)−O(7)	110.31(18)
O(3)−Co(2)−O(8f)	172.73(18)	O(6d)−S(2)−O(5)	108.51(17)
O(3)−Co(2)−O(9)	96.01(14)	O(6)−S(2)−O(5)	108.51(17)
O(8f)−Co(2)−O(9)	81.45(14)	O(7)−S(2)−O(5)	110.5(2)
O(3)−Co(2)−O(1a)	83.62(14)	Co(1)−O(8)−Co(2g)	125.86(13)
O(8f)−Co(2)−O(1a)	100.13(14)	Co(1)−O(8)−Co(2 h)	125.86(13)
O(9)−Co(2)−O(1a)	169.46(18)	Co(2g)−O(8)−Co(2 h)	97.96(18)
O(3)−Co(2)−O(6e)	94.11(15)	Co(1)−O(9)−Co(2)	118.93(15)
O(8f)−Co(2)−O(6e)	92.61(15)	Co(1)−O(9)−Co(2d)	118.93(15)
O(9)−Co(2)−O(6e)	88.10(15)	Co(2)−O(9)−Co(2d)	94.72(18)

[a] Symmetry codes: (a) $x, -y + 1, z - 1/2$; (b) $x + 1/2, -y + 1/2, z - 1/2$; (c) $-x + 1/2, -y + 3/2, z - 1/2$; (d) $-x, y, z$; (e) $-x, -y, z - 1/2$; (f) $-x, -y + 1, z - 1/2$; (g) $x, -y + 1, z + 1/2$; (h) $-x, -y + 1, z + 1/2$.

valence sum calculations[26] [Co(1) = 2.00 and Co(2) = 1.94] and the values of the bond distances indicate the valence state of both Co atoms to be +2. Interestingly, the Co atoms are bridged by μ_3-hydroxides to form a helical $Co_3(OH)_2$ ferrimagnetic chain (antiferromagnetic, Co(1) and Co(2); ferromagnetic, two Co(2) sites) (Figure 1b).[27] In **1**, the edge- or corner-sharing of $Co(1)O_6$, $Co(2)O_6$, and SO_4 polyhedra results in two-dimensional anionic $[Co_3(OH)_2(SO_4)_3(H_2O)_2]^{2-}$ layer in which the interchain shortest Co···Co distance over O−S−O bridge is 5.78 Å (Figure 1c). The anionic $[Co_3(OH)_2(SO_4)_3(H_2O)_2]^{2-}$ layers are linked by sodium ions via Na−O bonds into a three-dimensional neutral structure (Figure 1d).

Compound **2** also crystallizes in orthorhombic space group $Cmc2_1$ and the asymmetric unit consists of two Co(II) ions, two hydroxides, one hydrosulfate, half-sulfate and two water molecules as shown in Figure 1e. The assignment of hydrosulfate is required by charge balance. The Co(1) and S(2) atoms are located in the special positions. The Co(1) site adopts an octahedral geometry, coordinated by two hydroxides and four oxygen atoms from three sulfates. The Co(1)−O distances are in the range of 2.084(3)−2.174(4) Å. The cis and trans O−Co(1)−O angles are in the range of 77.83(16)−96.68(16)° and 166.17(16)−176.50(17)°, respectively. The Co(2) site also adopts an octahedral geometry, coordinated by two hydroxides, three oxygen atoms from three sulfates, and one water molecule. The Co(2)−O distances are in the range of 2.072(3)−2.148(3) Å. The cis and trans O−Co(1)−O angles are in the range of 82.68(14)−99.77(15)° and 169.80(15)−173.09(15)°, respectively. Similar to **1**, the helical ferrimagnetic $Co_3(OH)_2$ chain is formed in **2**. Because of the absence of sodium ions, the edge- or corner-sharing of $Co(1)O_6$, $Co(2)O_6$, HSO_4 and SO_4 polyhedra results in two-dimensional neutral $[Co_3(OH)_2(HSO_4)_2(SO_4)(H_2O)_2]$ layer (see Figure 1c). The adjacent layers are packed in AB fashion and the water molecules are filled between adjacent layers (see the Supporting Information, Figure S2).

Magnetic Properties. The temperature dependence of the magnetic susceptibility for **1** and **2** in the temperature range 2–300 K under a 1000 Oe applied field was studied with in a Quantum Design SQUID MPMS XL-7. The $\chi_m T$ value at 300 K is 10.18 cm^3 K mol^{-1} for **1** and 9.30 cm^3 K mol^{-1} for **2**, and decreases with lowering temperature down to a minimum value of 7.07 cm^3 K mol^{-1} at 80 K for **1** and 5.42 cm^3 K mol^{-1} at 70 K for **2** (Figure 2). Upon further cooling, the $\chi_m T$ value rapidly increases to a maximum of 340.90 at 30 K for **1** and 228.04 at 23 K for **2**, and then decreases to 26.40 for **1** and 12.93 for **2** at 2 K. The fitting of Curie–Weiss law in the temperature range 90–300K gives C = 12.70 cm^3 K mol^{-1}, θ = −71.2 K for **1**, and C = 10.44 cm^3 K mol^{-1}, θ = −70.9 K for **2**. The C values in **1** and **2** correspond to the effective magnetic moment 5.82 μ_B and 5.28 μ_B per Co, which are higher than the expected spin-only value of 3.87 μ_B for a high spin Co(II) ion, attributed to well documented orbital contribution. Neglecting the magnetic superexchange over three-atom bridges, hydroxide bridged Co−O chain is mainly responsible for the magnetic behavior. The superexchange topology of Co sites in the Co−O chain is shown in the Supporting Information, Chart S1. To simulate the magnetic behavior of **1** and **2**, we need a three-coupling-constant model. However, because the Co(1)···Co(2) distances over O(8) and O(9) sites (3.675 and 3.607 Å) are approximately equal, it is rational to approximately assume $J_1 = J_2$. The three-coupling-constant model is simplified as two-coupling-constant model (see the Supporting Information, Chart S2). The spin Hamiltonian expression is

$$\hat{H} = -2J\sum_i^n S_{Co,i}(S_{Co,i+1,up} + S_{Co,i+1,down}) - J'\sum_i^n S_{Co,i+1,up}S_{Co,i+1,down}$$

where J is the intrachain coupling between Co1 and Co2 and J' is the intrachain coupling between Co2 ions. To the best of our knowledge, there is lack of an analytical expression for such a two-coupling-constant model. Co1 and Co2 atoms over a single-hydroxide bridge have a larger Co···Co distance of 3.6 Å, whereas Co2 and Co2 atoms over a double-hydroxide bridge have a shorter Co···Co distance of 3.1 Å. Thus one may expect that J' is much larger than J and classic spin S = 3 is first formed by two ferromagnetic $Co(2)O_6$ octahedra. Therefore, regular ferrimagnetic chain is formed.

$$\hat{H} = -2J\sum_i^n S_{Co,i}(S_{Co,i+1,up} + S_{Co,i+1,down}) = -2J\sum_i^n S_{Co,i}S'_{Co,i+1}$$

where $S'_{Co,i+1} = S_{Co,i+1,up} + S_{Co,i+1,down} = 3$.

Correcting spin–orbital coupling and interchain antiferromagnetic coupling by θ,[28] the analytic expression for the above regular ferrimagnetic chain is available.[29]

$\chi = N\beta^2 g^2 S(S+1)/3k(T-\theta)\left(g^2(1+u)/(1-u) + \delta^2(1-u)/(1+u)\right)$

$u = \coth(x) - 1/x$, $x = J^e/kT$

$g = (g_a^e + g_b^e)/2$, $\delta = (g_a^e - g_b^e)/2$

$g_a^e = g_a\sqrt{S_a(S_a+1)}$, $g_b^e = g_b\sqrt{S_b(S_b+1)}$

$J^e = J\sqrt{S_a(S_a+1)S_b(S_b+1)}$

$S_a = 3/2$; $S_b = 3$

Assuming $g_a = g_b$, and fixing θ = −10 K, the best fitting (solid line) gives J = −9.2(1) cm^{-1}, $g_a = g_b$ = 2.52(1), $R = 9.8 \times 10^{-6}$ for **1**, and J = −9.0(1) cm^{-1}, $g_a = g_b$ = 2.28(1), $R = 4.0 \times 10^{-6}$, $R = [(\chi_m T)_{obsd} - (\chi_m T)_{calcd}]^2/[(\chi_m T)_{obsd}]^2$.

Preliminary measurements on field-dependent magnetization, field-cooled magnetization, and ac magnetic susceptibility show that **1** and **2** have similar magnetic behavior (Figures 2−7 and the Supporting Information, Figures S3–S5), and thus only **1** was further studied in detail. Field-cooled magnetizations of **1** in 500–50000 Oe applied dc fields show abrupt increase below 38 K (Figure 3), indicating the onset of spontaneous magnetization. The saturation effect can be clearly seen below 20 K. The magnetization of **1** at 2 K first

(26) Brown, I. D.; Altermatt, D. *Acta Crystallogr., Sect. B* **1985**, *41*, 244.
(27) Livage, C.; Egger, C.; Ferey, G. *Chem. Mater.* **1999**, *11*, 1546.

Table 3. Bond Lengths (Å) and Angles (deg) for 2[a]

Co(1)−O(2a)	2.084(3)	Co(2)−O(1c)	2.072(3)
Co(1)−O(2)	2.084(3)	Co(2)−O(8d)	2.100(3)
Co(1)−O(8)	2.100(4)	Co(2)−O(3)	2.103(3)
Co(1)−O(9)	2.102(4)	Co(2)−O(9)	2.111(3)
Co(1)−O(7b)	2.173(5)	Co(2)−O(6b)	2.121(3)
Co(1)−O(5)	2.174(4)	Co(2)−O(1W)	2.148(3)
S(1)−O(4)	1.455(3)	S(2)−O(6)	1.473(3)
S(1)−O(1)	1.467(3)	S(2)−O(6a)	1.473(3)
S(1)−O(3)	1.473(3)	S(2)-O(7)	1.476(5)
S(1)−O(2)	1.483(3)	S(2)−O(5)	1.477(4)
O(2a)−Co(1)−O(2)	166.17(16)	O(1c)−Co(2)−O(8d)	95.79(13)
O(2a)−Co(1)−O(8)	91.59(10)	O(1c)−Co(2)−O(3)	85.31(11)
O(2)−Co(1)−O(8)	91.59(10)	O(8d)−Co(2)−O(3)	173.09(15)
O(2a)−Co(1)−O(9)	96.74(8)	O(1c)−Co(2)−O(9)	169.80(15)
O(2)−Co(1)−O(9)	96.74(8)	O(8d)−Co(2)−O(9)	83.38(12)
O(8)−Co(1)−O(9)	89.52(16)	O(3)−Co(2)−O(9)	96.75(12)
O(2a)−Co(1)−O(7b)	88.01(10)	O(1c)−Co(2)−O(6b)	82.68(14)
O(2)−Co(1)−O(7b)	88.01(10)	O(8d)−Co(2)−O(6b)	99.77(15)
O(8)−Co(1)−O(7b)	176.50(17)	O(3)−Co(2)−O(6b)	87.14(13)
O(9)−Co(1)−O(7b)	93.98(16)	O(9)−Co(2)−O(6b)	87.43(14)
O(2a)−Co(1)−O(5)	83.11(8)	O(1c)−Co(2)−O(1W)	92.43(13)
O(2)−Co(1)−O(5)	83.11(8)	O(8d)−Co(2)−O(1W)	89.21(14)
O(8)−Co(1)−O(5)	98.68(16)	O(3)−Co(2)−O(1W)	83.92(13)
O(9)−Co(1)−O(5)	171.80(17)	O(9)−Co(2)−O(1W)	97.72(15)
O(7b)−Co(1)−O(5)	77.83(16)	O(6b)−Co(2)−O(1W)	170.14(13)
Co(2e)−O(8)−Co(2f)	93.32(16)	Co(1)−O(9)−Co(2a)	120.33(13)
Co(2e)−O(8)−Co(1)	125.92(12)	Co(1)−O(9)−Co(2)	120.33(13)
Co(2f)−O(8)−Co(1)	125.92(12)	Co(2a)−O(9)−Co(2)	92.67(16)

[a] Symmetry codes: (a) $-x, y, z$; (b) $-x, -y, z - 1/2$; (c) $x, -y + 1, z - 1/2$; (d) $-x, -y + 1, z - 1/2$; (e) $x, -y + 1, z + 1/2$; (f) $-x, -y + 1, z + 1/2$.

increases slowly with increasing field and then shows a sharp transition to a saturated value of 3.3 Nβ, consistent with the ferrimagnetic value per Co_3 unit (Figure 4). Interestingly, **1** exhibits a stepped hysteresis loop at 2 K with a coercive field of 1800 Oe and remnant magnetization of 2.8 Nβ (Figure 5). Similar stepped hysteresis loop is also discovered in cobalt-radical single-chain magnet [Co(hfacac)$_2$-(NITPhOMe)],[3] and authors pointed out that this reversible steps in the hysteresis loop arises from the different anisotropy axes of Co(II) spins in the helical chain. Field-cooled magnetization (FCM) and zero-field-cooled magnetization (ZFCM) measurements under an applied field of 100 Oe show the irreversibility below ca. 28 K, which is defined as the blocking temperature (Figure 6). The temperature dependence of the ac susceptibilities for **1** in zero applied static field with an oscillating field of 5 Oe and frequencies of 1, 10, 100, 300 and 997 Hz was studied. As shown in Figure 7, both real χ' and imaginary χ'' components in the ac susceptibility show frequency dependent maxima. This fact indicates a cooperative freezing of individual magnetic moments, characteristic of spin-glasses, superparamagnets or single-chain magnets.[28] The frequency dependence of real χ' component of ac susceptibility was studied by equation $\varphi = \Delta T_f/[T_f \Delta(\log \omega)]$, where T_f is the freezing temperature and ω is the frequency, and the estimated value of φ for **1** is 0.02, which is close to normal value for spin glass.[30] However, the Arrhenius law $\tau = \tau_0 \exp(-U/k_B T)$ (τ is the relaxation time, τ_0 is the pre-exponential factor, and U is the energy gap) holds and the fitting gives a set of parameters: $\tau_0 = 1.1 \times 10^{-6}$ s and $U/k_B = 129$ K (Figure 8). The resultant τ_0 seems a little larger but the U/k_B is normal for a typical SCM following Glauber dynamics. This dependence on frequency can also be fitted by the conventional critical scaling law of the spin dynamics (Figure 9), as described by $\tau = \tau_0 (T_p - T_f/T_f)^{-z\nu}$, giving $\tau_0 = 1.49 \times 10^{-3}$ s, $-z\nu = 3.3$, and $T_f = 8.9$ K (T_f is the critical temperature for a spin glass phase), the obtained $-z\nu$ value is out of the range (from 4 to 12) for various spin glasses.[30]

To investigate the magnetic behavior of **1**, we can fit the experimental data to 45 K using the non-critical-scaling theory with the following simple phenomenological equation[31]

$$\chi_m T = C_1 \exp(\alpha J/k_B T) + C_2 \exp(\beta J/k_B T)$$

where $\alpha J < 0$ indicates the antiferromagnetic interaction within the chain, which is responsible for the initial high temperature decay of $\chi_m T$. $\beta J > 0$ denotes the ferromagnetic-like interaction, which leads to the increase in $\chi_m T$ below 80 K. $C_1 + C_2$ roughly equals the Curie constant at high temperatures. The best fit gives $C_1 = 12.35$, $\alpha J/k_B = -60.2$ K, $C_2 = 0.072$, and $\beta J/k_B = 226.6$ K (Figure 10).

The plot of $d\log(T)/d\log(\chi T)_{ferro}$ versus T is shown in Figure 11. Here $(\chi T)_{ferro} = \chi_m T - 12.35 \times \exp(-60.2/T)$ describes the ferromagnetic contribution, which is obtained by subtracting the antiferromagnetic component that dominates at the high temperature regime from the total $\chi_m T$. As can be seen, the data in the temperature window from 35 to 120 K show nearly a straight line that roughly intersects the

(28) Kumagaia, H.; Okab, Y.; Inouea, K.; Kurmoo, M. *J. Phys. Chem. Solids* **2004**, *65*, 55.
(29) Kahn, O. *Molecular Magnetism*; Wiley−VCH: Weinheim, Germany, 1993.
(30) Mydosh, J. A. *Spin Glasses: An Experimental Introduction*; Taylor & Francis, London, 1993.
(31) *Magnetism: Molecules to Materials*; Miller, J. S., Drillon, M., Eds.; Wiley−VCH: Weinheim, Germany, 2005; Vol. 5, Chapter 10, p 347.

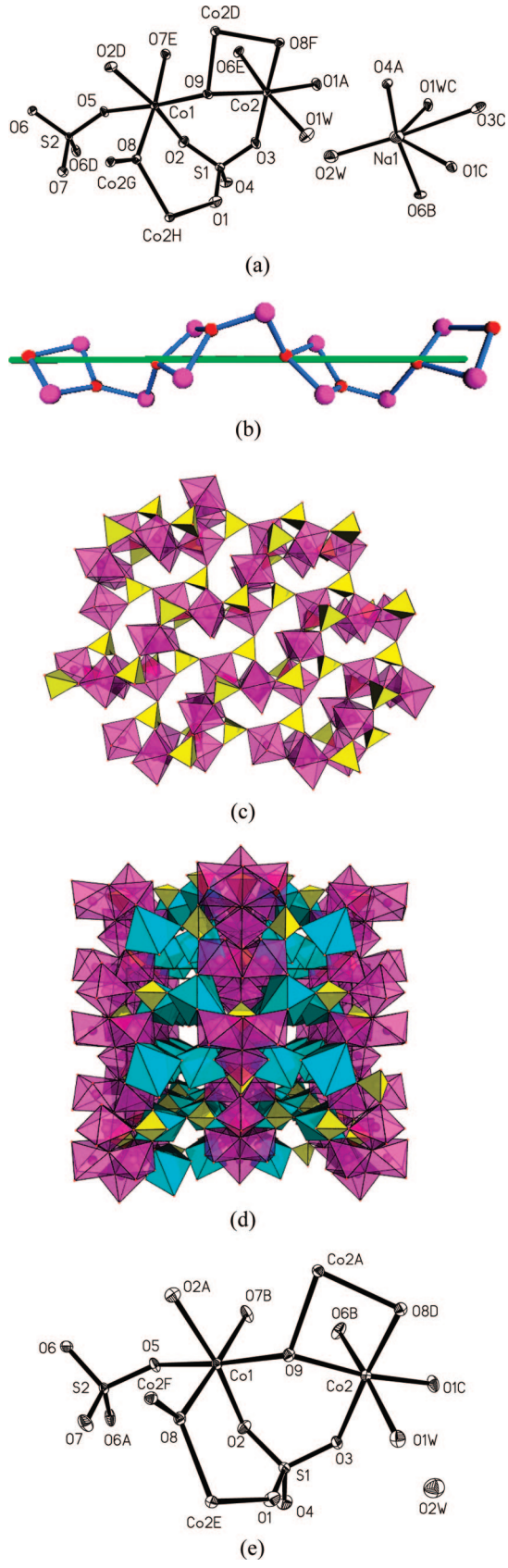

Figure 1. (a) Coordination environments of Co sites; (b) $Co_3(OH)_2$ helical chain; (c) polyhedral view of two-dimensional anionic $[Co_3(OH)_2(SO_4)_3(H_2O)_2]^{2-}$layer; (d) polyhedral view of three-dimensional structure formed by connection of $[Co_3(OH)_2(SO_4)_3(H_2O)_2]^{2-}$layers via sodium ions in **1**; (e) the coordination environments of Co sites in **2**. The Co, S, and Na are shown in purple, yellow, and blue octahedra, respectively.

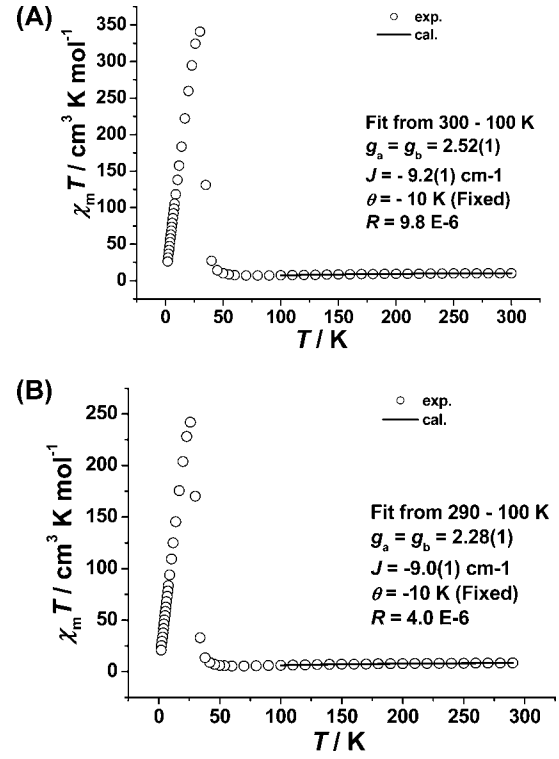

Figure 2. Measured (cycle) and fitted (line) $\chi_m T$ versus T curve per Co3 unit for **1** (a) and **2** (b) recorded at a field of 1000 Oe.

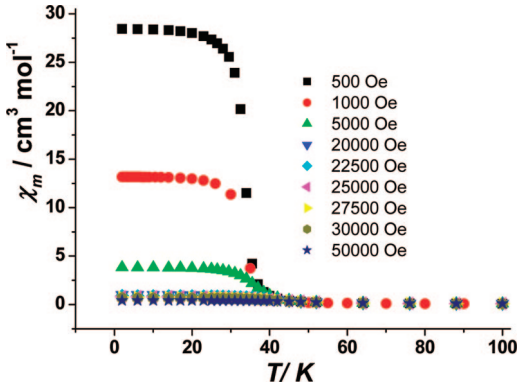

Figure 3. Field-cooling magnetization of **1** under various applied fields.

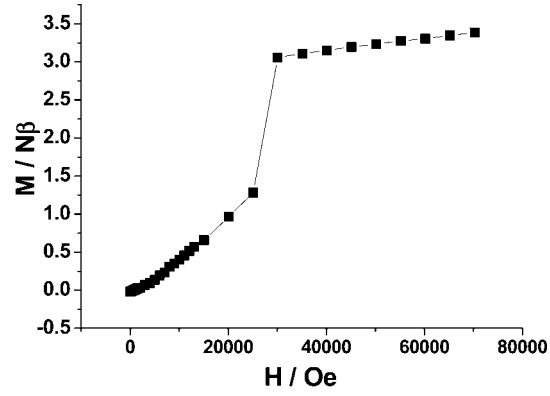

Figure 4. M versus H curve of **1**.

horizontal coordinate axes at the origin. This behavior may rule out the phase transition to long-range ordering of this system above 0 K, and suggests that **1** is indeed a real 1D system.[17,31]

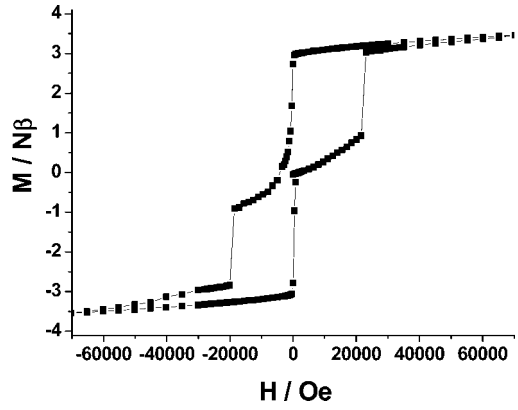

Figure 5. Magnetic hysteresis loop of **1** recorded at 2 K.

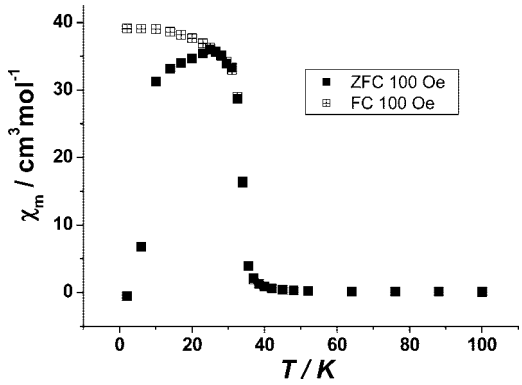

Figure 6. Field-cooling (FC) and zero-field-cooling (ZFC) magnetization of **1**.

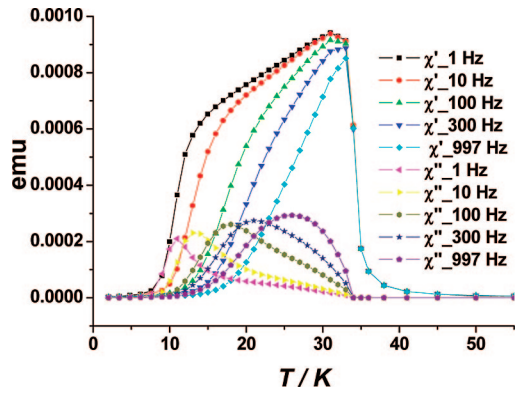

Figure 7. Frequency dependence of the ac susceptibility of **1** measured at H_{ac} = 5 Oe.

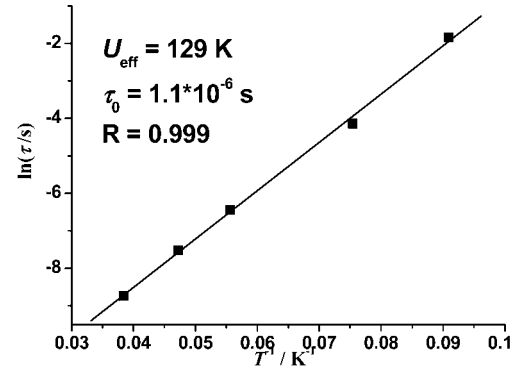

Figure 8. Frequency dependence of ac χ_m'' for **1** was fitted by Arrhenius law $\tau = \tau_0 \exp(-U/k_BT)$.

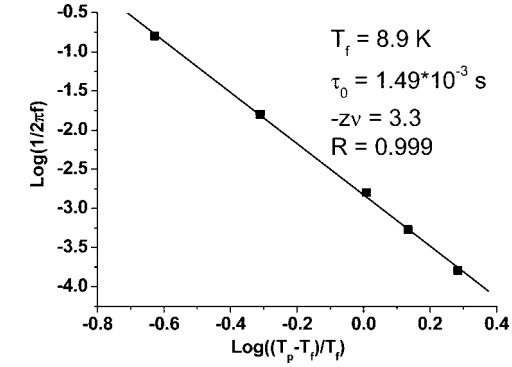

Figure 9. Frequency dependence of ac χ_m'' for **1** was fitted by the conventional critical scaling law of the spin dynamics as described $\tau = \tau_0 (T_p\text{-}T_f/T_f)^{-z\nu}$.

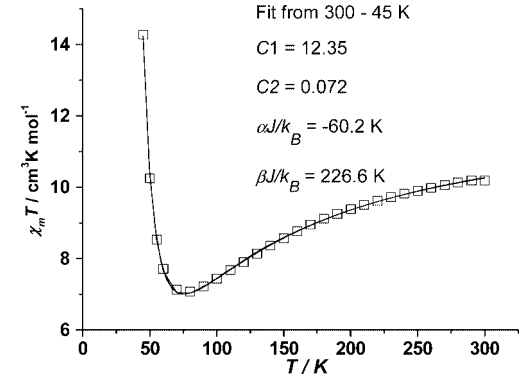

Figure 10. Fitting of experimental data using the non-critical-scaling theory with the following equation $\chi_m T = C_1 \exp(\alpha J/k_BT) + C_2 \exp(\beta J/k_BT)$.

Thermal Properties. Thermogravimetric analysis for **1** and **2** in air atmosphere and under 1 atm. pressure at the heating rate of 10 °C min^{-1} was performed on a polycrystalline samples. As shown in Figure 12, the initial weight loss of 14.8% (calcd 14.6%) in the temperature range of 170–450 °C corresponds to the removal of five water molecules (four water molecules from **1** itself and the fifth water being the product of reaction: $2OH^- = H_2O + O^{2-}$). The intermediate possibly has the empirical formula $Na_2Co_3O(SO_4)_3$. The XRPD pattern of the intermediate shows that it is noncrystalline (see the Supporting Information, Figure S6). No weight loss occurs in the temperature range of 450–710 °C, indicating that the intermediate is stable. The second weight loss of 23.2 (calcd 23.1%) in the temperature range of 710–980 °C is in agreement with the decomposition of two SO_4^{2-} sulfate groups as SO_3. The final residue at 980 °C is 62.0%, which is poorly crystalline mixture of Na_2SO_4 and CoO confirmed by XRPD patterns (see the Supporting Information, Figure S7).

$$Na_2Co_3(OH)_2(SO_4)_3(H_2O)_4 \rightarrow Co_3(SO_4)_3 + 5H_2O$$

$$Na_2Co_3O(SO_4)_3 \rightarrow Na_2SO_4 + 3CoO + 2SO_3$$

As shown in Figure 12, the initial weight loss of 20.8% (calcd 18.8%) in the temperature range of 260–400 °C corresponds to the removal of six water molecules (four water molecules from **2** itself and the other two being the product of hydroxide and proton). The XRPD pattern of a sample heated at 500 °C for 30 min shows that the intermediate is

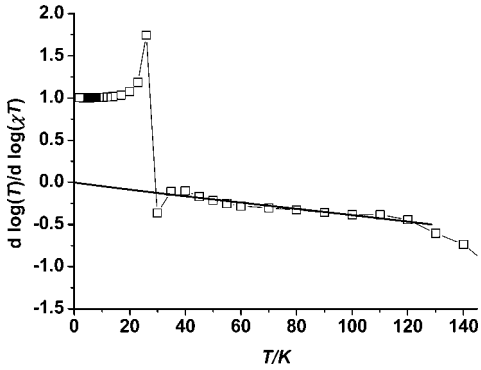

Figure 11. Plot of $d\log(T)/d\log(\chi_m T)_{ferro}$ versus T in **1**. $(\chi_m T)_{ferro}$ has been obtained by subtracting from the total $\chi_m T$, the antiferromagnetic component, which dominates at high temperature regime.

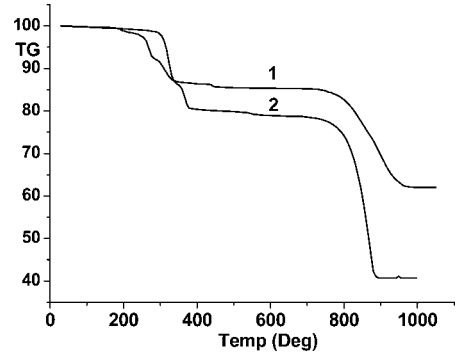

Figure 12. TGA curve of **1** in air stream at the heating rate of 10 °C/min.

poorly crystalline beta-$CoSO_4$ (see the Supporting Information, Figure S8). No weigh loss occurs in the temperature range of 550–710 °C. The second weight loss of 38.1% in the temperature range of 710–900 °C is in agreement with the decomposition of two SO_4^{2-} groups sulfates as SO_3. The final residue of 41.1% (calcd 41.8%) is poorly crystalline Co_3O_4 indicated by XRPD patterns (see the Supporting Information, Figure S9).

$$Co_3(OH)_2(HSO_4)_2(SO_4)(H_2O)_4 \rightarrow Co_3(SO_4)_3 + 6H_2O$$

Conclusion

Two helical $Co_3(OH)_2$ chain-based cobalt hydroxysulfates have been structurally determined using single-crystal X-ray diffraction. Preliminary temperature dependence of the magnetic susceptibility, field-dependence of magnetization, field-cooled magnetization, and ac magnetic susceptibility measurements show that **1** and **2** have similar ferrimagnetism and slow magnetic relaxation. **1** reveals a stepped hysteresis loop at 2 K with a coercive field of 1800 Oe and remnant magnetization of 2.8 Nβ attributed to the different anisotropy axes of Co(II) spins in the $Co_3(OH)_2$ helical chain. Field-cooled magnetization and zero-field-cooled magnetization measurements show blocking temperature of **1** ca. 28 K. The study of frequency dependence by equation $\varphi = \Delta T_f/[T_f\Delta(\log \omega)]$ shows magnetic behavior of **1** is close to a spin glass. However, the Arrhenius law holds and the fitted U/k_B is normal for a typical SCM following Glauber dynamics. The obtained $z\nu$ value by the conventional critical scaling law of the spin dynamics $\tau = \tau_0(T_p - T_f/T_f)^{-z\nu}$ is out of the range for various spin glasses. The plot of $d\log(T)/d\log(\chi T)_{ferro}$ versus T eliminates the phase transition to long-range ordering and suggests that **1** is a real 1D system. Compound **1** is tentatively ascribed to be a ferrimagnetic chain with unusual spin-glass-like dynamic relaxation. The usual slow relaxation behavior possibly arises from the movement of the domain walls.

Acknowledgment. This work was financially supported by NSFC (20771069), NECT (05–0270), and FANEDD (200422).

Supporting Information Available: Crystal structural data for **1** and **2** (CIF); XRPD and additional figures (PDF). This material is available free of charge via http://pubs.acs.org.

CM7032542